Journal of Science and Technology in Civil Engineering, HUCE, 2026, 20 (3): 146–164

PINEAPPLE LEAF CONVERSION TO NANOCELLULOSE FIBER AND ITS IMPACT ON THE POROSITY, MECHANICAL STRENGTH, AND MICROSTRUCTURE OF CEMENT-BASED COMPOSITES

Trong-Phuoc Huynh[a,*], Dan-Thuy Van-Pham[b], Hong Truong Anh[b], Huynh Cong Ly[b], Nguyen Minh Tri[b]

[a]*Faculty of Civil Engineering, College of Engineering, Can Tho University, Campus II, 3/2 Street, Ninh Kieu Ward, Can Tho City, Vietnam*
[b]*Faculty of Chemical Engineering, College of Engineering, Can Tho University, Campus II, 3/2 Street, Ninh Kieu Ward, Can Tho City, Vietnam*

Article history:
Received 23/10/2025, Revised 05/1/2026, Accepted 03/3/2026, Available online 25/9/2026, Version of Record 25/9/2026

Abstract

The growing demand for sustainable and low-carbon construction materials underscores the importance of developing cementitious composites (CCs) that utilize renewable waste-derived admixtures without sacrificing performance. This study examines the effects of nanocellulose fibers (NF) extracted from pineapple leaf waste–a largely untapped agricultural byproduct–on the mechanical, microstructural, and porosity characteristics of CCs containing Class-F fly ash. CC samples incorporating 0.0–2.0 wt.% NF were evaluated for compressive and flexural strengths, porosity, and microstructural evolution using FTIR, XRD, and SEM analyses. The results revealed that a small addition of 0.5 wt.% NF helped maintain hydration uniformity and retained about 90% of the control compressive strength (74.1 MPa → 66.7 MPa), while higher dosages caused substantial deterioration: compressive and flexural strengths decreased to 10.2 MPa and 2.3 MPa, respectively, corresponding to an approximately 86% reduction in strength and a 253% increase in porosity (10.44% → 36.85%). A strong inverse, nonlinear correlation between porosity and mechanical strength was identified, confirming porosity as the principal factor governing performance. Overall, pineapple leaf–derived NF serves as a promising eco-efficient additive at low concentrations, but excessive dosages lead to agglomeration, hindered hydration, and pore coarsening, emphasizing the need for optimized dispersion and dosage control in bio-based fiber–reinforced cement systems. These findings provide insights for the sustainable design of eco-efficient CCs.

Keywords: cement-based composites; mechanical strength; microstructure; nanocellulose fiber; pineapple leaves; porosity.

1. Introduction

The urgent need for sustainable construction materials has driven extensive research into bio-based reinforcements for cementitious composites (CCs). Cement production alone contributes approximately 7–8% of global CO_2 emissions [1], while conventional concrete formulations consume vast quantities of natural resources. To address these challenges, eco-friendly alternatives–such as mineral replacements (e.g., fly ash [FA], slag [2]) and renewable reinforcements derived from natural fibers–have emerged as viable strategies to reduce the environmental footprint of concrete without

*Corresponding author. *E-mail address:* htphuoc@ctu.edu.vn (Huynh, T.-P.)
https://doi.org/10.31814/stce.huce2026-20(3)-08 p-ISSN 1859-2996; e-ISSN 2734-9268
© 2026 The Author(s). Published by Hanoi University of Civil Engineering. Licensed under CC BY-NC-ND 4.0.

compromising mechanical strength or durability. Among these alternatives, natural fibers obtained from agricultural residues have shown substantial potential as sustainable reinforcements [3]. Unlike synthetic fibers, plant-based fibers are biodegradable, cost-effective, and widely available. Recent advancements in natural fiber–reinforced CCs have demonstrated marked improvements in mechanical, thermal, and durability performance. Particularly, nanocellulose extracted from agricultural byproducts such as pineapple leaf fiber [4] and bemban fibers has gained increasing attention due to its high aspect ratio, crystallinity, and renewability.

Nanocellulose-reinforced cement systems have exhibited significant improvements in structural performance. Rahmawati et al. [5] incorporated 0–3 wt.% bemban fiber nanocellulose (BFNC) into CCs and reported that 1 wt.% BFNC increased compressive strength by 9.38%, while enhancing thermal stability and microstructural compactness. Similarly, Cherian et al. [6] successfully extracted nanocellulose fiber from pineapple leaf (PALF) using steam explosion and acid hydrolysis, producing nanoscale fibrils with high crystallinity and surface reactivity, which are compatible with cement hydration and pore refinement processes. Investigations into macro-scale natural fibers further emphasize the importance of surface modification. Pereira et al. [7] treated PALF with tannic acid (2–10%) following NaOH pre-treatment and observed that a 3 wt.% fiber content improved both workability and mechanical performance. In a related study, Kueh et al. [8] incorporated silica aerogel into PALF-reinforced composites and found that 0–2% PALF mitigated strength reduction caused by lightweight fillers while improving acoustic insulation and flexural strength. Hybrid and polymer-modified systems have also demonstrated favorable outcomes. Hancharoen et al. [9] combined oil palm fibers with waste tire rubber, resulting in a 10% increase in flexural strength, an 85% reduction in water absorption, and enhanced thermal insulation. Likewise, Demirdağ et al. [10] reported that coconut fiber reinforced with polymer binders achieved superior interfacial bonding and mechanical strength compared to glass fibers, highlighting the critical role of interfacial morphology in fiber–matrix interaction.

Recent state-of-the-art reviews on natural fiber-reinforced cementitious matrix composites provide a useful benchmark for interpreting the present results. Common natural fibers such as coir, flax, jute, sisal, bagasse, and hemp generally exhibit densities in the range of about 1.05–1.6 g/cm^3 and tensile strengths from roughly 150 up to 1800 MPa, values that are lower than those of E-glass fibers but still sufficient to enhance toughness and tensile response when properly dispersed in cementitious matrices. At the composite scale, these reviews indicate that relatively low natural fiber dosages (around 0.03–0.5% by volume) can reduce density and, in some cases, increase compressive and tensile strength by approximately 5–30%, whereas higher fiber fractions often reduce workability, increase porosity, and impair compressive strength because of fiber clustering and insufficient fiber–matrix contact [11].

Within this broader context, pineapple-leaf-derived nanocellulose fibers (NFs) can be viewed as part of the natural-fiber family in terms of their potential to modify the physical and mechanical behaviour of cement-based composites. However, the present study shows that the beneficial range for NFs is very narrow: low dosages can slightly refine the pore structure and maintain mechanical performance, while higher dosages ($\geq$ 1.0 wt.%) lead to a marked increase in porosity and a substantial loss of strength. This dosage-sensitive response is consistent with previous observations on natural fibers, reinforcing the idea that waste-derived NF cannot be assumed to act as an effective reinforcement at arbitrary contents, and that careful control of fiber dosage, dispersion, and surface condition is essential to achieve performance comparable to other natural fiber-reinforced cementitious systems.

From a durability perspective, Song et al. [12] applied ZrO_2 coatings to natural fibers, which im-

proved alkali resistance and mechanical stability under accelerated aging conditions, offering valuable insights into long-term performance. These findings collectively highlight that durability performance in natural fiber–modified cementitious composites depends strongly on fiber surface chemistry, water absorption behavior, and the resulting modification of pore connectivity. Surface-modified fibers tend to enhance long-term stability by reducing alkali-induced degradation and limiting internal microcracking, whereas untreated natural fibers may impair durability due to swelling, delayed hydration, and increased pore continuity. Choi [13] and Lee and Choi [14] further demonstrated that excessive water uptake by plant-based fibers can elevate internal porosity and facilitate carbonation or moisture transport, thereby reducing resistance to long-term chemical and physical deterioration. This contrast underlines an important durability-based research gap: although NF offers high aspect ratio and reactivity, its influence on hydration uniformity, pore refinement, and long-term stability (especially when blended with FA) remains insufficiently clarified. In terms of thermal performance, Wijesinghe et al. [15] demonstrated that the addition of 0.5 vol.% elastane (12 mm) textile fibers to cementitious composites reduced thermal conductivity by 62% while maintaining a compressive strength of 39.65 MPa, indicating the dual advantage of mechanical reinforcement and thermal insulation.

Although previous studies have confirmed the reinforcing potential of nanocellulose and natural fibers, most research focuses on macrofibers or generic cellulose rather than pineapple leaf–derived nanocellulose integrated with pozzolanic binders. The influence of such nanofibers on pore structure, hydration processes, and long-term durability remains insufficiently understood. Pineapple leaf, a high-cellulose-content byproduct of tropical fruit cultivation, is often discarded or incinerated, contributing to agricultural waste. Utilizing this resource for material production not only offers a value-added application but also aligns with circular economy principles. Accordingly, this study investigates the effect of pineapple leaf–derived NF on the porosity, mechanical strength, and microstructure of FA-modified CCs by varying NF content from 0.0 to 2.0 wt.% and performing mechanical, porosity, FTIR, XRD, and SEM analyses. The main objective is to identify dosage thresholds and mechanistic effects of NF incorporation, rather than to optimize load-bearing performance; the upper dosage of 2.0 wt.% is included specifically to capture the full response range of the system. This allows the identification of the critical fiber content beyond which excessive water absorption, inadequate dispersion, and hydration interference lead to significant increases in capillary porosity and loss of matrix densification. Such high-dosage mixtures are evaluated solely to define performance limits and to clarify the mechanisms governing NF–cement interactions, rather than as recommended practical proportions. The findings will contribute to the rational design of greener, fiber-reinforced binders that integrate renewable nanomaterials into modern cement systems, while also addressing the balance between sustainability, workability, and mechanical integrity in nanocellulose-reinforced composites.

Despite the promising outcomes reported for various plant-based fibers, a clear gap remains in understanding how NFs extracted from pineapple leaf biomass interacts with cement–FA blended systems, particularly in terms of pore evolution, hydration uniformity, and performance thresholds. Moreover, previous studies often relied on either commercially sourced NF or chemically intensive extraction methods, leaving limited insight into fibers produced through milder, more sustainable routes. The present study addresses these gaps by employing NFs synthesised entirely in-house from pineapple leaves using an eco-optimized protocol, and systematically evaluating its effects across a wide dosage range (0–2.0 wt.%). By identifying the transition from beneficial internal curing at low NF levels to severe porosity-driven deterioration at higher dosages, this work provides new mechanistic understanding and establishes critical design limits for integrating waste-derived NFs into

FA-modified CCs.

2. Fabrication of nanocellulose fiber from pineapple leaves

Pineapple leaves, a locally abundant agricultural waste byproduct, were collected, thoroughly washed, sun-dried, and mechanically shredded to facilitate subsequent chemical processing (Fig. 1). The shredded material was first soaked in hot water to remove surface impurities and extractable compounds. Following this pre-treatment, 20 g of the dried biomass underwent an alkaline treatment using sodium hydroxide (NaOH, 2 wt.%) at 100 °C for 4 hours [16]. This step effectively removed lignin and hemicellulose fractions by disrupting intermolecular hydrogen bonds. The treated material was then rinsed repeatedly with distilled water until a neutral pH (pH = 7) was achieved.

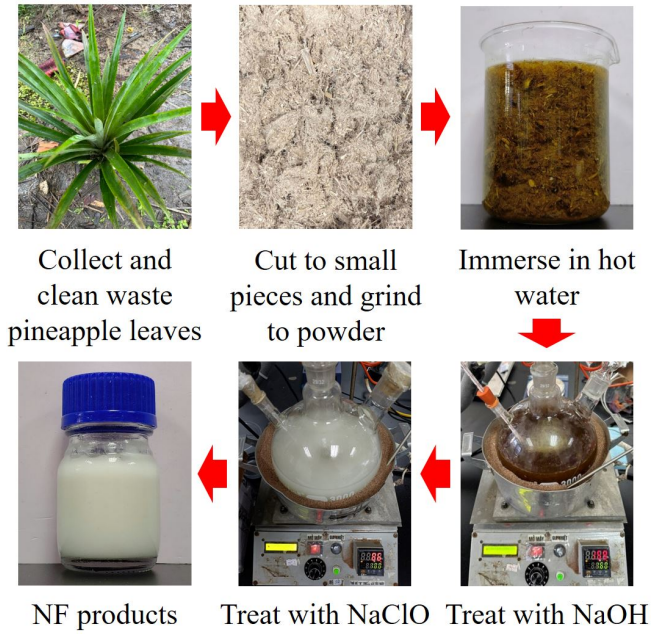


Figure 1. Procedures of NF fabrication

Subsequently, the delignified fibers were bleached using sodium hypochlorite (NaClO, 4 wt.%) at 80 °C under continuous stirring for 4 hours. During this stage, a small amount of acetic acid (CH_3COOH) was added to enhance the oxidation of residual chromophoric groups. As reported by Thien et al. [16], elevated NaClO concentrations may alter the fiber length and diameter of the resulting cellulose, an effect later confirmed through transmission electron microscopy (TEM) imaging (as shown later in Fig. 5). After bleaching, the sample was centrifuged and washed with deionized water until the pH stabilized at neutrality. The nanocellulose fabrication procedure (Fig. 1) was adapted from the method established by Lam et al. [17], with minor modifications. The process involved sulfuric acid hydrolysis (H_2SO_4, 64 wt.%) conducted at 45 °C for a specified reaction period, followed by neutralization, centrifugation, and purification. The resulting NFs exhibited high crystallinity and thermal stability, confirming their suitability as reinforcing agents for sustainable cementitious composites. It is important to clarify that all NFs used in this study were synthesized directly by the authors in-house; no pre-fabricated or previously produced fibers were utilized. Instead, the entire extraction route, including alkaline delignification, NaClO bleaching, and sulfuric acid hydrolysis, was performed in-house, following and refining the protocol established in our earlier publication [16, 17]. The NFs incorporated in the mixtures were therefore freshly prepared specifically for this experimental program.

Although NF fabrication typically involves several chemical stages, the procedure adopted in this work was deliberately kept mild. Both the alkaline treatment (2 wt.% NaOH) and bleaching step (4 wt.% NaClO) were performed under moderate temperatures, following eco-optimized protocols reported in recent studies. These conditions reduce chemical consumption compared with conventional extraction routes, while the use of pineapple leaves, an agricultural residue without cultivation inputs, further limits the environmental footprint of the process. The synthesized NFs displayed nanoscale diameters of approximately 10–35 nm, high aspect ratio, and an interconnected fibrillar network, as evidenced by the TEM images (as shown later in Fig. 5). These characteristics align with the mechanical performance reported for acid-hydrolyzed NF in literature, where tensile strengths frequently reach several gigapascals. Although direct tensile testing of individual fibrils was not performed here, these benchmark values help contextualize the reinforcing potential of the NFs used in this study, which was beyond the scope of the present work.

3. Materials and experimental methods

3.1. Materials

The primary binder used in this study was Portland cement (specific gravity of 3.07), classified as grade 40 (PC40), conforming to the Vietnamese standard TCVN 2682:2020 [18], which specifies consistent quality in terms of fineness, chemical composition, and compressive strength development. Fly ash (FA), classified as Class F according to TCVN 10302:2014 [19], was obtained from a Southern thermal power plant of Vietnam. The FA, with a specific gravity of 2.27, was employed as a partial cement replacement to improve sustainability and enhance the reactivity of the binder system. The chemical compositions of cement and FA are summarized in Table 1.

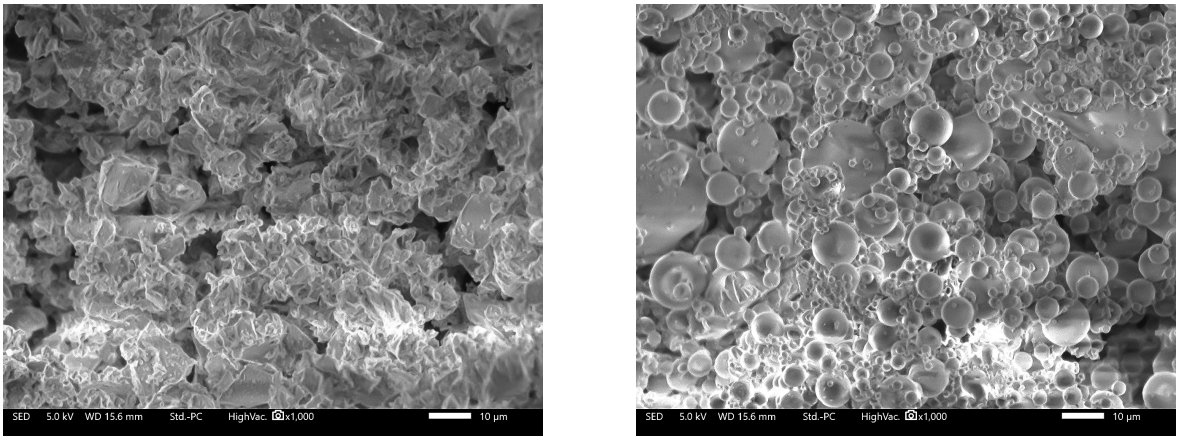
Table 1. Chemical compositions of binder materials

Chemical elements (wt.%)	Cement	Fly ash
SiO_2	18.2	62.0
Al_2O_3	3.0	20.8
Fe_2O_3	4.3	9.1
CaO	69.6	2.3
MgO	0.9	-
SO_3	2.8	0.5
K_2O	0.6	2.8
Na_2O	-	0.5
Others	0.6	2.0

As shown in Table 1, the cement primarily consists of CaO (69.6 wt.%), accompanied by moderate amounts of SiO_2 (18.2 wt.%), Fe_2O_3 (4.3 wt.%), and Al_2O_3 (3.0 wt.%), which are typical of Ordinary Portland Cement. In contrast, the FA exhibits a markedly different composition, dominated by SiO_2 (62.0 wt.%) and Al_2O_3 (20.8 wt.%), with a relatively low CaO content of 2.3 wt.%, thereby confirming its classification as a Class F pozzolan as aforementioned. The high silica and alumina contents of the FA contribute to its pozzolanic reactivity, promoting the formation of secondary calcium silicate hydrate (C–S–H) phases when blended with cement. Minor constituents such as SO_3, K_2O, and Na_2O are also present in trace quantities and may influence parameters such as setting behavior, sulfate resistance, and overall durability.

The morphology and mineralogical characteristics of the binder components were examined using scanning electron microscopy (SEM), Fourier-transform infrared spectroscopy (FTIR), and X-ray

diffraction (XRD). As depicted in Fig. 2, SEM micrographs reveal that cement particles exhibit angular and irregular morphologies, which enhance mechanical interlocking and bonding efficiency within the cementitious matrix. In contrast, the FA particles appear predominantly spherical and smooth, a morphology that improves workability and packing efficiency through the well-known ball-bearing effect [20, 21].



(a) Cement (b) FA

Figure 2. SEM images of cement and FA

Fig. 3 presents the FTIR spectra of cement and FA, highlighting the principal functional groups within the wavenumber range of 4000–400 cm^{-1}. Both materials exhibit broad absorption bands between 3840 and 3610 cm^{-1}, corresponding to O–H stretching vibrations attributed to hydroxyl groups and adsorbed moisture [22, 23]. In the cement spectrum, absorption peaks at 1697, 1506, and 1425 cm^{-1} are associated with H–O–H bending and carbonate vibrations [23], indicating partial carbonation and the presence of calcite. Prominent Si–O stretching modes appear at 1113 and 887 cm^{-1} [24], whereas low-frequency bands at 673 and 527 cm^{-1} correspond to Al–O and Si–O bending vibrations characteristic of hydrated cement phases such as calcium silicate hydrate (C–S–H) and calcium aluminate hydrate (C–A–H) [25, 26]. For FA, a dominant peak centered at 1074 cm^{-1} represents the asymmetric stretching of Si–O–Si bonds in the amorphous aluminosilicate glassy phase. Additional peaks at 812 and 467 cm^{-1} correspond to mullite and quartz, respectively [27]. These spectral features confirm the chemical reactivity and mineralogical composition of both binders, with FA exhibiting pronounced pozzolanic potential owing to its high content of amorphous silicate structures.

Fig. 4 illustrates the XRD patterns of cement and FA, recorded over a 2θ range of 10°–70°. The cement sample exhibits well-defined crystalline peaks at 29.14°, 32.05°, and 34.17°, corresponding to alite (C_3S) and belite (C_2S), which are the principal clinker phases responsible for early- and long-term strength development [28]. Additional diffraction peaks observed at 25.12°, 42.84°, and 51.54° are attributed to gypsum and calcite, confirming minor sulfate and carbonate phases within the cement [29]. In contrast, the FA sample displays distinct diffraction peaks at 26.28°, 30.69°, 34.92°, and 38.99°, characteristic of crystalline quartz and mullite phases [30]. The broad background hump centered around 20°–35° further indicates the presence of an amorphous aluminosilicate glassy phase, which contributes to its pozzolanic reactivity. These XRD profiles collectively highlight the high reactivity of cement clinker minerals and the role of FA as a supplementary pozzolanic material capable of enhancing long-term strength and microstructural refinement in blended cementitious systems.

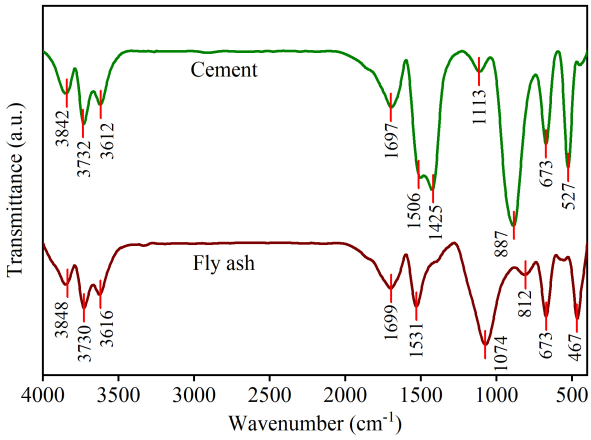


Figure 3. FTIR spectra of cement and FA

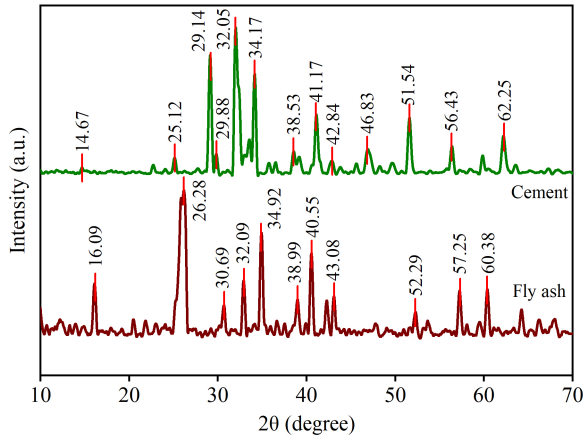


Figure 4. XRD patterns of cement and FA

Fig. 5 presents transmission electron microscopy (TEM) micrographs of NFs synthesized from pineapple leaf biomass. The fibers exhibit a highly entangled, web-like morphology, consisting primarily of elongated and flexible fibrils. Occasional spherical particles are observed, which may indicate localized aggregation or incomplete hydrolysis during the acid treatment process. The uniform nanoscale diameters and fibrillar network confirm the successful defibrillation of cellulose microfibrils achieved through the sulfuric acid hydrolysis procedure.

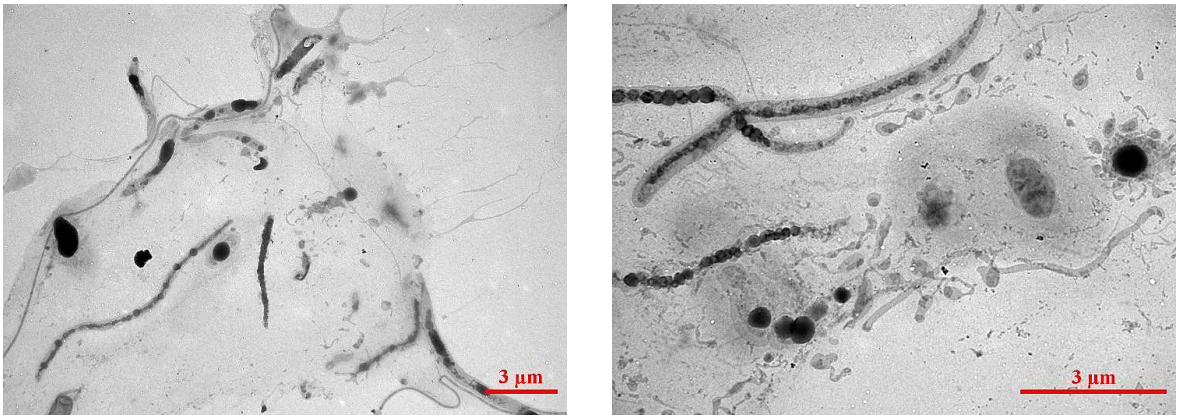


Figure 5. TEM observation of synthesized NFs

Fig. 6 illustrates the FTIR spectra of synthesized NFs subjected to sequential chemical treatments, including hot-water extraction, alkaline treatment with NaOH, and bleaching with NaClO. The initial spectrum of the hot-water–treated sample displays prominent absorption bands at approximately 1728 cm^{-1}, 1514 cm^{-1}, and 1246 cm^{-1}, which correspond to the C=O stretching vibrations of hemicellulose ester linkages [31], the aromatic skeletal vibrations of lignin, and the C–O stretching modes in lignin and hemicellulose, respectively [32]. These characteristic peaks are substantially diminished or completely absent following the subsequent NaOH and NaClO treatments, confirming the effective removal of hemicellulose and lignin from the biomass. Concurrently, a progressive increase in transmittance intensity is observed at around 3340 cm^{-1} and 2900 cm^{-1}, associated with O–H and C–H stretching vibrations, respectively, indicating the enrichment of cellulose within the treated fibers [33]. The emergence of sharp bands near 896 cm^{-1}, assigned to β-glycosidic linkages characteristic of cellulose, further validates the isolation of high-purity cellulose fibers [34]. These spectral

transitions collectively verify the effectiveness of the chemical purification sequence, consistent with prior findings by Thien et al. [16] and Zheng et al. [35]. The results affirm that pineapple leaves constitute a promising and renewable source of nanocellulose with high purity and structural integrity suitable for reinforcing sustainable cementitious composites.

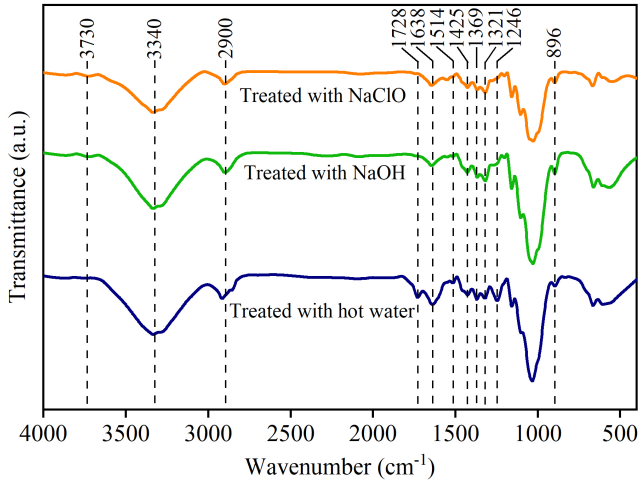


Figure 6. FTIR spectra of synthesized NFs

The fine aggregate used in this study was natural river sand sourced from local construction material suppliers in Southern Vietnam. Its particle characteristics satisfied the grading and quality requirements for fine aggregates used in concrete production. A polycarboxylate-based superplasticizer (SP) was employed as a high-range water-reducing admixture. Potable tap water was used for all mixing and curing processes.

3.2. Mixture proportions and samples preparation

The mix proportions for the cementitious composites (Table 2) were developed based on the mix design framework proposed by Alzoubi et al. [36], with modifications introduced to align with the objectives of this study. A constant water-to-binder (w/b) ratio of 0.25 was maintained to ensure low water demand and minimize internal porosity. The binder system consisted of 85 wt.% cement and 15 wt.% FA, selected for its pozzolanic reactivity and contribution to long-term strength development. The sand-to-binder ratio was fixed at 1.0 across all mixtures to maintain a consistent aggregate content throughout the experimental program. To ensure comparable workability among all mixtures, SP was incorporated at a dosage of 1.2 wt.% of the total binder. The dosage was optimized through preliminary trials to achieve a target flow spread diameter of 25 ± 2 cm, consistent with the requirements for self-compacting or highly flowable cementitious composites. All mixtures incorporating different NF dosages met this target flow range, indicating that fixing SP at 1.2 wt.% was sufficient to maintain the required workability without causing fiber-induced loss of flowability or segregation. NFs were added to the mixtures at varying dosages of 0.5, 1.0, 1.5, and 2.0 wt.% relative to the total binder mass (cement + FA). The control mixture (NF0.0) contained no NF addition. Table 2 summarizes the detailed mix proportions of each formulation, expressed in weight percentages, allowing for a direct comparison of binder composition, NF dosage, and admixture content used in this study.

All components listed in Table 2 were thoroughly blended using a laboratory-scale pan mixer to ensure homogeneous dispersion of NFs within the cementitious matrix. First, dry materials (cement, FA, sand, and NFs) were blended for 2 minutes to ensure uniform dispersion. Water and SP were then gradually added, and mixing continued for an additional 3 minutes until a homogeneous mixture

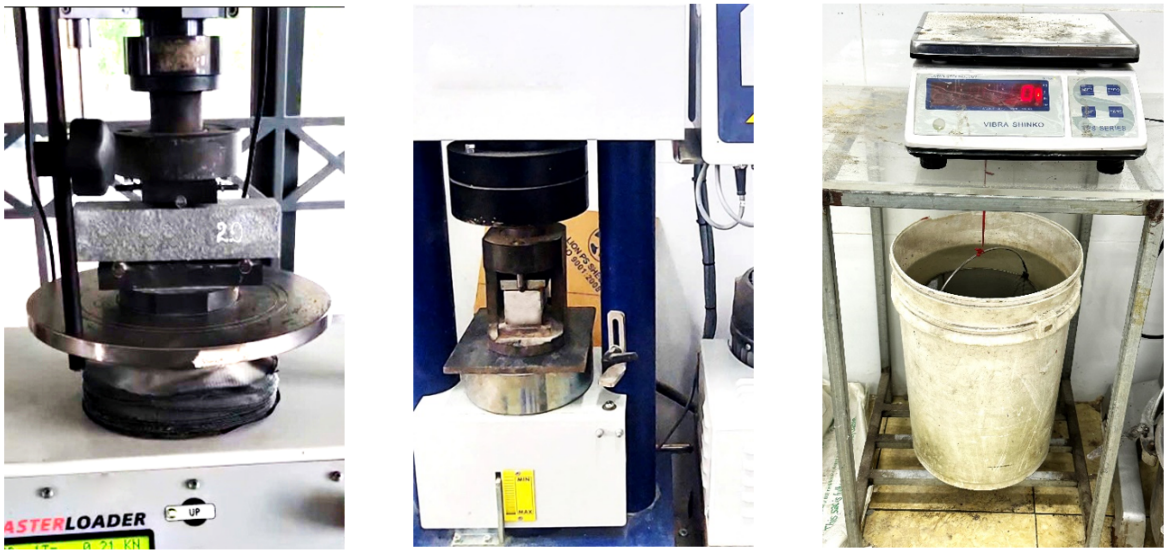
was achieved. The resulting fresh CC mixture was cast into molds of various sizes depending on the target tests. After casting, the specimens were covered to minimize moisture loss and cured under controlled laboratory conditions until the designated testing ages.

Table 2. Material proportions of CC samples

Mixtures	Binder (wt.%)		Sand/binder ratio (by weight)	Water/binder ratio (by weight)	NF (wt.% of binder)	SP (wt.% of binder)
	Cement	FA				
NF0.0	85	15	1.0	0.25	0.0	1.2
NF0.5	85	15	1.0	0.25	0.5	1.2
NF1.5	85	15	1.0	0.25	1.5	1.2
NF2.0	85	15	1.0	0.25	2.0	1.2

3.3. Test methods

Flexural strength was determined using prism specimens with dimensions of $40 \times 40 \times 160$ mm after 7 and 28 days of curing (Fig. 7(a)), following the procedure outlined in ASTM C348-21 [37]. Compressive strength was evaluated on the two broken halves of each prism after flexure (Fig. 7(b)) in accordance with ASTM C349-18 [38]. For both tests, the reported strength values represent the average of three replicate specimens to ensure statistical reliability and reproducibility.



(a) Flexural strength (b) Compressive strength (c) Porosity

Figure 7. Test methods used to determine the CC's properties

Total porosity of the hardened CCs was measured using the mass-based suspension–saturation–drying procedure following the method previously adopted by Nguyen et al. [39]. For each mixture, $50 \times 50 \times 50$ mm cubes were immersed in water for 24 h then obtain the suspension mass (M_{sus}) as shown in Fig. 7(c). After wiping surface water, the saturated mass (M_{sat}) was recorded. The specimens were then oven-dried at 105 ± 5 °C until constant mass to obtain the dry mass (M_{dry}). Total porosity (P, %) was calculated according to Eq. (1):

$$P(\%) = \left(\frac{M_{\text{sat}} - M_{\text{dry}}}{M_{\text{sat}} - M_{\text{sus}}}\right) \times 100\%. \quad (1)$$

This approach captures the accessible pore volume associated with water intrusion and is consistent with established porosity characterisation protocols in alkali-activated and blended binder systems.

To analyze the functional groups and chemical evolution of the CCs, FTIR analysis was performed using a Shimadzu IRAffinity-1S WL spectrometer. The spectra were recorded in the wavenumber range of 4000–400 cm^{-1} to identify the organic and inorganic bond vibrations associated with hydration products and NFs interactions. Besides, XRD analysis was conducted to investigate the mineralogical phases present in the cement matrix. The measurements were carried out using a BRUKER diffractometer equipped with CuKα radiation, operating at a scanning rate of 0.02° s^{-1} over a 2θ range of 10°–70°. The analysis was used to identify crystalline hydration products and unreacted phases. Furthermore, the microstructure and morphology of the hardened composites were examined using SEM observations. Fractured samples obtained after compressive strength testing were analyzed with a JEOL JCM-7000 microscope to observe fiber dispersion, matrix densification, and interfacial bonding between the NFs and cementitious phases.

4. Results and discussion

4.1. Porosity

Fig. 8 presents the porosity results of CCs containing varying NF dosages derived from pineapple leaf waste. The control sample (NF0.0), which contained no NF, exhibited the lowest porosity at 10.44%, reflecting a dense microstructure with minimal pore connectivity. As the NF content increased, a progressive rise in porosity was observed, reaching 14.16% (NF0.5), 22.07% (NF1.0), 30.67% (NF1.5), and 36.85% (NF2.0). Compared to the control, the porosity of the NF2.0 mixture increased by approximately 253%, demonstrating a positive correlation between NF dosage and matrix porosity. This trend can be attributed to a combination of synergistic and competing mechanisms.

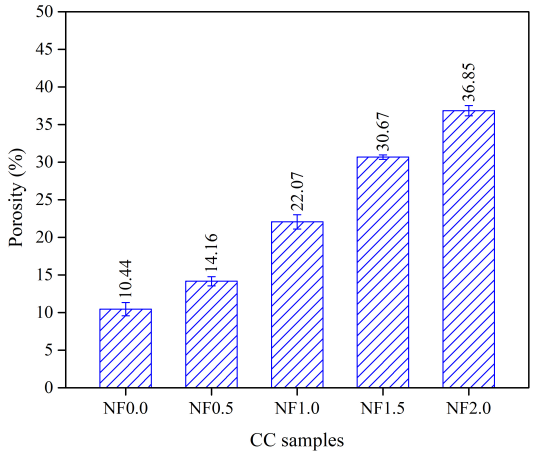


Figure 8. Porosity of CC samples

At low dosages (≤ 0.5 wt.%), NFs may assist moisture redistribution and localized internal curing, leading to slightly improved hydration uniformity. However, when the NF content exceeds 1.0 wt.%, excessive fiber addition may cause agglomeration and interfere with cement hydration, disrupting the formation of a continuous calcium silicate hydrate (C–S–H) network and generating interconnected microvoids. The hydrophilic surface functional groups of NFs increase water demand during mixing, which can lead to entrapped air and higher total porosity if not adequately compensated by SP dosage. These findings align well with those reported by Alzoubi [36], who observed that while low NF dosages enhance matrix densification and hydration efficiency, excessive fiber content promotes porosity due to fiber clustering, poor dispersion, and impaired bonding within the cementitious matrix. The porosity evolution observed in this study is also consistent with the dosage-dependent

effects documented in previous natural-fiber and nanocellulose research. In systems incorporating hydrophilic plant-based fibers, porosity typically increases once the fiber content surpasses the optimal threshold due to excess water uptake, fiber agglomeration, and incomplete hydration. Choi [13] reported that plant-derived fibers accelerate internal curing at low dosages but progressively elevate pore connectivity as fiber concentration increases, an effect directly mirrored in the transition from 10.44% porosity in NF0.0 to 22.07% and 30.67% in the NF1.0 and NF1.5 mixtures, respectively. Likewise, Rahmawati et al. [5] observed that nanocellulose additions above 1 wt.% disrupt the continuity of hydration products, producing porous zones comparable to the highly coarsened structure measured at 36.85% porosity in the NF2.0 mixture of the present work. These earlier findings reinforce the interpretation that porosity in NF-modified CCs is governed not only by the intrinsic hydrophilicity of cellulose fibrils but also by their dispersion quality and influence on the local w/b ratio. At low dosage ($\leq$ 0.5 wt.% NF), the slight porosity increase corresponds to water retention that enhances localized hydration. However, beyond 1.0 wt.% NF, the sharp rise in porosity reflects the combined effects of fiber clustering, hindered C–S–H gel formation, and enlarged capillary void networks–mechanisms also evident in the SEM images presented in Section 4.5. Collectively, the comparison with previous studies shows that the porosity range measured here (10–37%) and its strong dependence on fiber dosage are consistent with established behaviour of natural fiber systems.

4.2. Mechanical strength

Fig. 9 illustrates the influence of NFs on the mechanical performance of CCs. A distinct inverse correlation was observed between NF content and both compressive (CS) and flexural strengths (FS). The control specimen (NF0.0) achieved the highest mechanical performance, with CS of 74.1 MPa and FS of 16.1 MPa, representing the fully hydrated, unmodified reference matrix. Upon incorporating 0.5 wt.% NF (NF0.5), both strength parameters exhibited reductions to 66.7 MPa (−10.0%) and 13.0 MPa (−19.3%) for CS and FS, respectively. This outcome suggests that at low dosages, NFs may function as a mild water-retaining agent, enhancing internal curing and maintaining microstructural integrity without significantly compromising the hydration network.

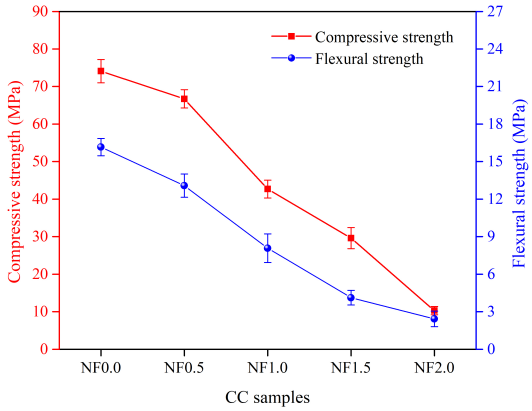


Figure 9. Mechanical strength of CC samples

A more pronounced strength decline was observed at 1.0 wt.% NF (NF1.0), where the CS decreased to 42.80 MPa (−42.2%), and FS dropped to 8.0 MPa (−50.3%) compared to the control. Further increases to 1.5 wt.% (NF1.5) and 2.0 wt.% (NF2.0) resulted in severe mechanical deterioration, with CS values of 29.50 MPa (−60.2%) and 10.20 MPa (−86.2%), and FS values of 4.0 MPa (−75.2%) and 2.3 MPa (−85.7%), respectively. These steep reductions clearly indicate that mechanical integrity is substantially compromised when NF dosage exceeds 1.0 wt.%. This deterioration mirrors the substantial increase in porosity from 10.44% in NF0.0 to 36.85% in NF2.0, representing an approximate 253% increase. Collectively, these results demonstrate that excessive NF content not only disrupts the C–S–H network but also generates interconnected voids, which act as stress concentrators responsible for the severe loss of structural capacity. This degradation in performance is primarily attributed to several interrelated mechanisms: (i) agglomeration of NF at higher concentrations produces weak zones that disrupt uniform stress transfer; (ii) the high water absorption capacity

of cellulose fibrils alters the effective water-to-cement ratio, leading to incomplete hydration; and (iii) the formation of fiber networks physically obstructs the development of the C–S–H gel, the principal load-bearing phase in cementitious materials. These findings are consistent with previous studies. Rahmawati et al. [5] reported that incorporating Bemban fiber nanocellulose above 1.0 wt.% in CCs led to diminishing mechanical performance due to fiber agglomeration and inadequate stress transfer. Similarly, Choi [13] noted that plant-based fibers, while beneficial at low dosages through internal curing, tend to delay hydration and reduce compressive strength as their content increases, primarily because of their high water absorption and interference with hydration kinetics. In the present study, the 86.2% loss in CS at 2.0 wt.% NF coincides with a 253% increase in porosity, confirming that excessive NF loading severely compromises both matrix densification and hydration efficiency.

Compared with systems using chemically modified or surface-treated NF (e.g., carboxylated or sulfonated NF), the performance decline observed here is more pronounced. This discrepancy can be attributed to the unmodified surface chemistry of the pineapple leaf–derived NF, which likely results in weak interfacial adhesion and limited chemical compatibility with cement hydration products. Poor bonding at the fiber–matrix interface serves as a potential crack initiation site under stress, further undermining mechanical reliability. In summary, while NFs extracted from pineapple leaf fiber show promise as a sustainable reinforcing additive, their dosage must be carefully optimized. Based on the combined mechanical, porosity, and microstructural results, the recommended practical dosage of pineapple-leaf-derived NF in FA-modified cementitious composites is $\leq$ 0.5 wt.% of binder, beyond which fiber agglomeration, increased porosity, and hydration disruption outweigh any potential internal curing benefits. A narrow beneficial window is observed at low NF dosages, where the benefits of internal curing are preserved without loss of structural cohesion. Beyond this threshold, adverse effects, including porosity increase, hydration disruption, and poor dispersion, dominate, emphasizing the need for optimized fiber surface modification and dispersion control in nanocellulose-reinforced cement systems.

It is important to note that the sharp decline in mechanical performance at higher NF dosages indicates that the untreated pineapple-leaf-derived NF used in this study does not behave as a conventional reinforcing nanofiber. Instead, once the dosage exceeds its workable dispersion limit, the NFs act more like impurities that interrupt hydration, elevate porosity, and destabilize the C–S–H network. This behaviour is consistent with the drastic increase in porosity (from 10.44% in NF0.0 to 36.85% in NF2.0) and the heterogeneous, highly porous microstructures observed in the SEM images (as shown later in Fig. 13). These findings do not contradict the purpose of the research but rather redefine its implications: the results establish a clear dosage threshold and reveal the mechanisms that prevent reinforcement effectiveness under untreated conditions. Such outcomes highlight the need for improved dispersion strategies or surface modification to unlock the potential of waste-derived NF. By identifying the limits and failure modes of the current approach, the study contributes essential insight into the design constraints and future development of sustainable NF-based additives. Accordingly, the CC mixtures containing 1.0–2.0 wt.% NF should be regarded as intentionally overdosed conditions used to define the upper performance boundary. Their behavior highlights how excessive NF disrupts hydration kinetics, weakens the interfacial transition zone (ITZ), increases connected porosity, and ultimately reduces load-bearing capacity. These mixtures serve as diagnostic tools for understanding material degradation mechanisms and for delineating the safe operational dosage window for NF-modified CCs.

When compared with those previous reports, the porosity range measured here (about 10–37%) and its strong coupling with mechanical properties indicate that NF behaves similarly to other natural

fiber systems, as it provides only a narrow beneficial dosage. Above this dosage, increased porosity and pore connectivity govern the response, outweighing any potential crack-bridging effect. This nonlinear decay trend and the narrow beneficial dosage window are consistent with previous reports on natural-fiber-reinforced systems, where porosity and pore connectivity rapidly dominate mechanical response once the fiber content exceeds the optimum [5, 11, 13]. Fig. 10 illustrates the relationship between porosity and the mechanical performance of NF-modified CCs, showing a clear nonlinear decay trend in which strength decreases rapidly as porosity increases. As the NF dosage increased, matrix porosity rose from 10.44% in the control mixture (NF0.0) to 36.85% in NF2.0–corresponding to a nearly 253% increase in internal voids. This substantial rise in pore volume aligns closely with the sharp reductions in both compressive strength (from 74.1 MPa to 10.2 MPa, −86.2%) and flexural strength (from 16.1 MPa to 2.3 MPa, −85.7%). The curvature of the trend in Fig. 10 reflects the accelerating influence of porosity on strength deterioration: small increases in porosity at low NF contents cause moderate strength loss, whereas higher porosity levels result in disproportionately greater reductions in load-bearing capacity.

The nonlinear nature of the correlation suggests that once porosity exceeds approximately 20–25%, the cement matrix enters a critical degradation zone where pore coalescence, capillary connectivity, and weakened ITZs significantly undermine structural integrity. This behavior is consistent with the microstructural observations, where excessive NF leads to fiber agglomeration, localized water depletion, hindered C–S–H gel formation, and the development of interconnected void networks. These defects serve as stress concentrators under loading, explaining the rapid decline in both compressive and flexural performance in high-porosity mixtures. Overall, the correlation shown in Fig. 10 confirms that porosity is the principal parameter governing the mechanical response of NF-modified CCs. The steep decay in strength with increasing porosity highlights the importance of optimizing NF dosage to avoid excessive fiber clustering and associated microstructural disruption. The trend also demonstrates that low NF dosages, which maintain porosity near the lower bound, preserve structural capacity, whereas higher dosages push the system into a pore-dominated failure regime. This relationship provides a robust basis for predicting performance and designing NF-reinforced composite mixtures with balanced strength and sustainability.

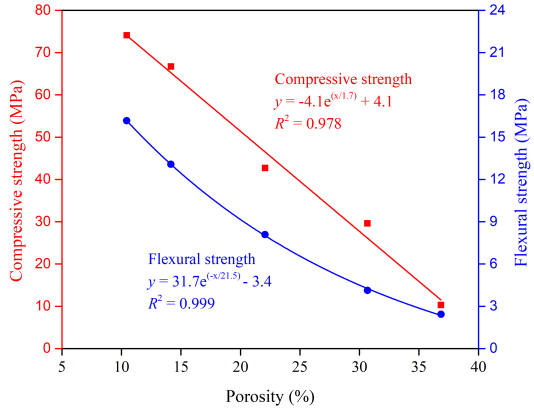


Figure 10. Correlation between porosity and mechanical strength of CC samples

4.3. FTIR analysis

Fig. 11 presents the FTIR spectra of CCs within the range of 4000–400 cm^{-1}. All specimens, including those incorporating NF, exhibited characteristic peaks corresponding to standard cement hydration products, similar to the control mix (NF0.0). However, variations in peak intensity and broadening indicate compositional and microstructural differences resulting from the inclusion of NF. The broad absorption band centered around 3614 cm^{-1} corresponds to the stretching vibration of hydroxyl groups (OH) primarily associated with calcium hydroxide [$Ca(OH)_2$], a key hydration product [23]. The intensity of this band typically increases with curing age as hydration progresses. In NF-containing composites, this band appears slightly broadened, which can be attributed to the

overlapping OH stretching of both bound water and the hydroxyl functionalities of the cellulose fibrils.

A weak band detected near 2981 cm^{-1} in higher NF dosages is associated with C–H stretching vibrations, indicating minor contributions from organic residues in the nanocellulose structure [40]. Meanwhile, the absorption peak around 1525 cm^{-1} corresponds to the asymmetric stretching of carbonate ions (CO_3^{2-}) [23], which is indicative of calcium carbonate ($CaCO_3$) formation through partial carbonation of portlandite during curing. This peak becomes slightly more pronounced with increasing NF content, likely due to the elevated porosity that facilitates CO_2 ingress and carbonation reactions. The strong and broad band centered near 1051 cm^{-1} is commonly associated with the asymmetric stretching of Si–O bonds within the C–S–H gel–the principal strength-contributing phase in hydrated cement [41]. Additionally, a distinct peak at 961 cm^{-1} is assigned to the asymmetric stretching of Si–O–Al or Si–O–Si linkages, typical of C–(A)–S–H gels in blended cement systems [25]. This suggests partial substitution of Al into the silicate network, consistent with the pozzolanic contribution of FA. The absorption peak near 779 cm^{-1} corresponds to the out-of-plane bending mode of CO_3^{2-} [25], confirming minor carbonation in all samples. Furthermore, bands in the 660–440 cm^{-1} region are attributed to bending vibrations of Si–O and Ca–O bonds [42], which are characteristic of crystalline hydration products and silicate frameworks.

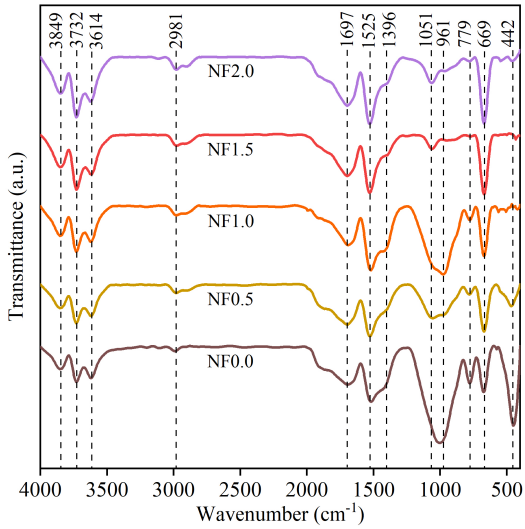


Figure 11. FTIR spectra of CC samples

Overall, the FTIR spectra confirm the presence of typical hydration phases (C–S–H, portlandite, and minor $CaCO_3$) in all mixtures. To avoid over-interpreting individual bands, these assignments are treated as qualitative indicators rather than definitive phase identifications. Accordingly, the discussion focuses on broader spectral changes, such as the relative broadening of O–H and Si–O regions, which more reliably reflect hydration evolution and the influence of NF on water retention and gel development. However, the variation in intensity and band broadening observed in NF-modified specimens indicates subtle changes in hydration dynamics, likely influenced by the water retention capacity, surface chemistry, and fiber–gel interactions of the NF. These spectroscopic observations are consistent with the previously reported differences in porosity and mechanical performance, particularly at higher fiber contents.

4.4. XRD analysis

Fig. 12 presents the XRD patterns of CCs containing varying dosages of NF. A prominent diffraction peak at $2\theta = 17.80°$, corresponding to portlandite [$Ca(OH)_2$] [43], is clearly observed across all samples. The intensity of this peak increases markedly with higher NF content, particularly in NF2.0, suggesting the accumulation of unreacted $Ca(OH)_2$. This trend likely reflects incomplete hydration, caused by excessive water absorption and hindered ion mobility arising from fiber clustering at elevated NF dosages. A distinct peak at $2\theta = 26.36°$, attributed to quartz (SiO_2) [44], appears consistently in all mixes with nearly unchanged intensity. This confirms the mineralogical stability of the FA and fine aggregate components, and indicates that NF incorporation did not alter the

crystalline silica content of the matrix. The strong diffraction peak centered around $2\theta = 29.13^{\circ}$, assigned to calcite ($CaCO_3$) [45], exhibits a noticeable increase in intensity for NF2.0. This suggests enhanced carbonation due to higher porosity and improved CO_2 diffusion within fiber-rich matrices. Conversely, the peak at $2\theta = 39.25^{\circ}$, also corresponding to calcite [46], shows a gradual decrease in intensity with increasing NF content, indicating that the polymorphic form or spatial distribution of the carbonation products may shift depending on matrix porosity and curing conditions. This contrasting trend among calcite-associated peaks may reflect differences in polymorph distribution or localized carbonation pathways within the more porous NF-rich matrices.

Interestingly, the diffraction signal near $2\theta = 49.96^{\circ}$, typically associated with a metastable polymorph of $CaCO_3$ [45], reaches its highest intensity at NF1.0 before diminishing at both lower and higher NF contents. These peak variations are interpreted cautiously, as XRD alone cannot confirm the formation of specific carbonation products or hydration phases. Therefore, the emphasis is placed on overall trends, such as the variations of portlandite intensity and changes in the amorphous hump, which more reliably indicate modified hydration progression and the microstructural influence of NF. Importantly, no new crystalline phases were detected upon NF incorporation. This finding indicates that NF does not alter the fundamental hydration chemistry of the cementitious system. Instead, its influence appears to be microstructural–modulating the morphology, porosity, and carbonation behavior of hydration products through its water-retention capacity and physical interaction with the developing gel network.

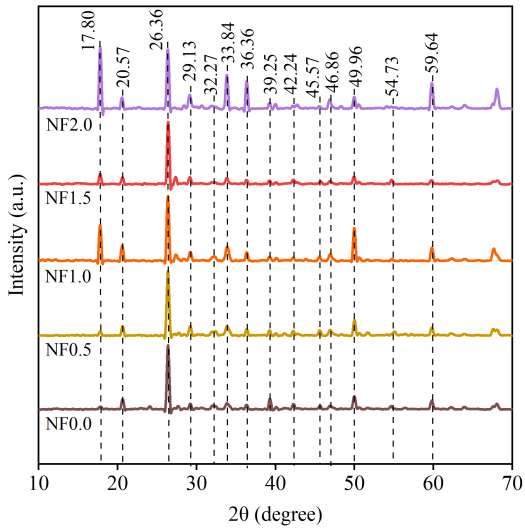
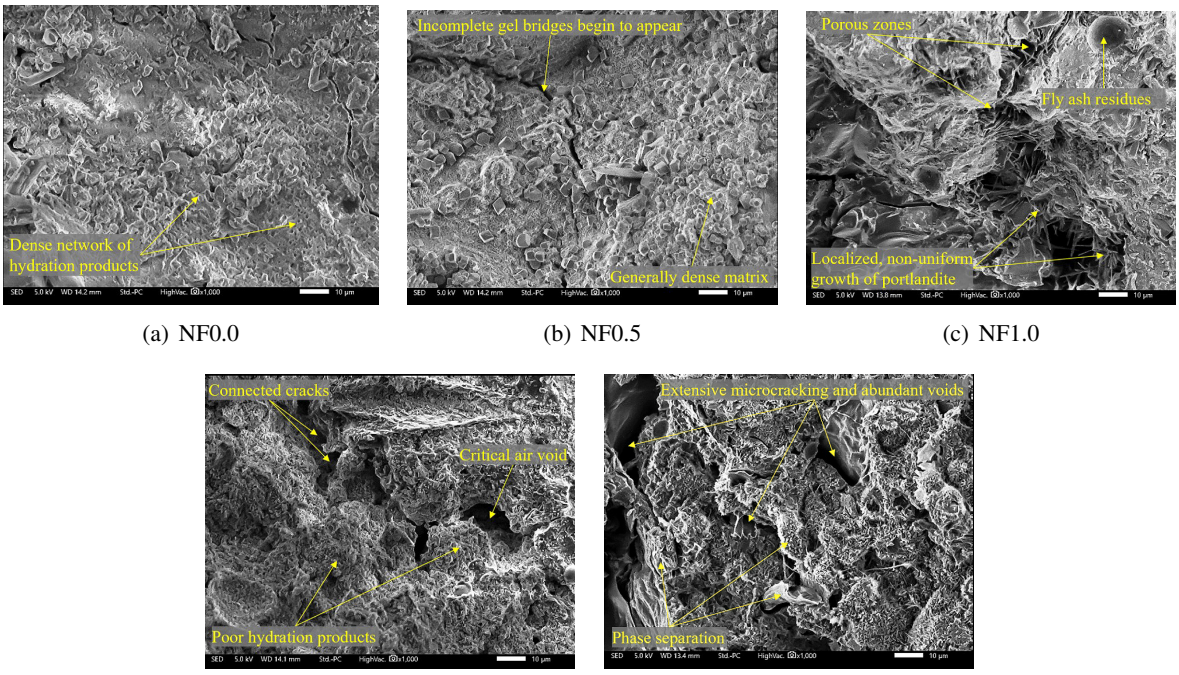


Figure 12. XRD patterns of CC samples

4.5. SEM observation

Fig. 13 presents the SEM micrographs of CC after 28 days of curing, revealing clear morphological variations in hydration products and matrix integrity as a function of NF content. In the control sample (Fig. 13(a)), the microstructure appears dense and homogeneous, characterized by a continuous network of hydration products, predominantly C–S–H gel and well-formed ettringite needles. The absence of visible cracks or major voids indicates a well-hydrated matrix, consistent with the superior mechanical strength observed earlier. The NF0.5 specimen (Fig. 13(b)) maintains a generally compact structure, although localized porosity and partially developed gel bridges begin to emerge. Some unreacted particles are visible, but the hydration products remain well connected, suggesting that a small amount of NF contributes a mild internal curing effect without severely hindering hydration reactions. At 1.0 wt.% NF (Fig. 13(c)), the microstructure becomes noticeably heterogeneous. Unhydrated cement grains, porous regions, and irregularly shaped FA residues are evident. The presence of large needle- and plate-like crystals suggests localized supersaturation and non-uniform precipitation of portlandite. These features indicate that excessive NF begins to disrupt hydration uniformity, likely due to its high water absorption and fiber agglomeration–consistent with the concurrent reduction in mechanical strength.



(a) NF0.0 (b) NF0.5 (c) NF1.0

(d) NF1.5 (e) NF2.0

Figure 13. SEM micrographs of CC samples

In the NF1.5 specimen (Fig. 13(d)), further deterioration of the matrix is apparent, with visible cracks and interconnected pores. The presence of poorly bonded hydration products and discontinuous gel phases implies that NF is not only altering water availability but also disturbing particle packing and cement-FA interactions, leading to diminished matrix cohesion. The most severe degradation is observed in NF2.0 (Fig. 13(e)), where the surface morphology is highly porous and fractured. Extensive microcracking, irregular voids, and loosely bound crystalline clusters dominate the structure. The observation of fibrous remnants and unreacted FA confirms that excessive fiber content consumes mix water and obstructs binder formation, resulting in incomplete hydration and phase separation. In particular, SEM images of NF1.5 and NF2.0 mixtures illustrate fiber-rich clusters and interconnected void networks, confirming that water absorbed by agglomerated NF disrupts the local w/b ratio and prevents the formation of a dense C–S–H matrix. These porous regions act as crack initiation sites, explaining the severe reduction in mechanical properties and supporting the porosity–strength correlations as above discussion. This microstructural disintegration also aligns closely with the drastic reductions in compressive and flexural strength reported earlier. Overall, the SEM observations confirm that moderate NF incorporation ($\leq$ 0.5 wt.%) preserves matrix integrity and may promote localized internal curing, whereas higher dosages ($\geq$ 1.0 wt.%) induce heterogeneous hydration, porosity, and cracking. These microstructural trends corroborate the FTIR, XRD, and mechanical test results, collectively underscoring the critical importance of dosage optimization in achieving balanced performance in NF-modified CCs. In this sense, excessive NF contents behave more like micro-impurities than reinforcements, as they introduce fiber-rich porous clusters that destabilize the load-bearing C–S–H network.

5. Conclusions

This study comprehensively evaluated the influence of pineapple leaf–derived NF on the mechanical, physical, and microstructural properties of CCs incorporating FA. Across five mixtures containing 0–2.0 wt.% NF, mechanical tests, porosity measurements, and microstructural analyses (FTIR, XRD, and SEM) consistently demonstrated that NF content plays a decisive role in governing hydration dynamics and overall performance.

- CS and FS decreased markedly with increasing NF content–from 74.1 MPa (NF0.0) to 10.2 MPa (NF2.0) and from 16.1 MPa to 2.3 MPa, respectively–corresponding to reductions of about 86.2% and 85.7%. Meanwhile, porosity rose from 10.44% to 36.85%, exhibiting a strong inverse, nonlinear correlation with strength: higher porosity levels led to disproportionately greater reductions in both compressive and flexural performance.

- FTIR and XRD analyses confirmed the presence of conventional hydration and carbonation products (C–S–H, $Ca(OH)_2$, and $CaCO_3$), yet peak broadening and reduced intensities in high-NF samples indicated suppressed hydration and enhanced carbonation due to water absorption and fiber agglomeration. SEM micrographs further revealed a transition from dense, cohesive matrices ($\leq$ 0.5 wt.% NF) to porous, cracked structures at higher dosages, with unreacted FA and incomplete gel formation.

- Collectively, these results suggest that while NFs may contribute to localized internal curing at low dosages and contribute to sustainability objectives, excessive incorporation ($>$ 0.5 wt.%) impairs hydration efficiency, increases porosity, and weakens structural integrity. An optimal dosage below 0.5 wt.% is therefore recommended to balance eco-efficiency with mechanical performance in NF-reinforced cementitious systems. Future studies may explore surface modification or dispersion enhancement to further optimize NF performance in cement-based systems.

Acknowledgement

We acknowledge Can Tho University (Vietnam) for supporting this study.

Declaration of generative AI and AI-assisted technologies

The author(s) declare that no generative AI or AI-assisted technologies were used in the preparation of this manuscript.

References

[1] Zheng, Y., Xi, X., Liu, H., Du, C., Lu, H. (2024). A review: Enhanced performance of recycled cement and CO_2 emission reduction effects through thermal activation and nanosilica incorporation. *Construction and Building Materials*, 422:135763.

[2] Huynh, T.-P., Ho, L. S., Ho, Q. V. (2022). Experimental investigation on the performance of concrete incorporating fine dune sand and ground granulated blast-furnace slag. *Construction and Building Materials*, 347:128512.

[3] Wang, X., Jin, Y., Ma, Q., Li, X. (2024). Performance and mechanism analysis of natural fiber-reinforced foamed concrete. *Case Studies in Construction Materials*, 21:e03476.

[4] Yadav, V. K., Verma, N., Kardam, S. K., Pullela, M. (2025). Pineapple leaf fiber in polymer composites: Structure, characterization, and applications. *Materials Chemistry and Physics: Sustainability and Energy*, 2:100011.

[5] Rahmawati, C., Faisal, M., Roslidar, Fitriani, Ahmad, J., Muliana, I. (2025). Extraction and characterization of nanocellulose from bemban fibre for cement-based composite. *Case Studies in Construction Materials*, 22:e04100.

[6] Cherian, B. M., Leão, A. L., De Souza, S. F., Thomas, S., Pothan, L. A., Kottaisamy, M. (2010). Isolation of nanocellulose from pineapple leaf fibres by steam explosion. *Carbohydrate Polymers*, 81:720–725.

[7] Amaral Pereira, I. D. S., Tostes Linhares Júnior, J. A., Fadini Natalli, J., Malafaia, S. A. A., Marvila, M. T., de Azevedo, A. R. D. (2024). Evaluation of the potential of treatments by NaOH and tannic acid of pineapple leaf (*Ananas comosus*) fiber used as reinforcement in coating mortars. *Journal of Building Engineering*, 95:110234.

[8] Kueh, A., Razali, A., Lee, Y., Hamdan, S., Yakub, I., Suhaili, N. (2023). Acoustical and mechanical characteristics of mortars with pineapple leaf fiber and silica aerogel infills - Measurement and modeling. *Materials Today Communications*, 35:105540.

[9] Hancharoen, K., Kamhangrittirong, P., Suwanna, P. (2024). Improvement of natural fiber cement composite for roofing applications through addition of waste tire rubber: An investigation of the physical, mechanical, thermal, and acoustic properties. *Cleaner Materials*, 13:100265.

[10] Demirdağ, C., Nodehi, M., Bideci, A., Bideci, Ö. S., Tuncer, M., Gencel, O., Ozbakkaloglu, T. (2024). The use of natural (coconut) and artificial (glass) fibers in cement-polymer composites: An experimental study. *Construction and Building Materials*, 412:134895.

[11] Do, N. T., Tran, M. T., Pham, D. T. (2023). State-of-the-art review of physical and mechanical properties of natural fibre-reinforced cementitious matrix composite. *Journal of Transport Science and Technology*, 12:49–63.

[12] Song, H., Liu, T., Gauvin, F., Brouwers, H. J. H. (2024). Evaluation of zirconia modification on the durability of natural fiber-reinforced cement composites using accelerated aging. *Journal of Building Engineering*, 84:108632.

[13] Choi, Y. C. (2022). Hydration and internal curing properties of plant-based natural fiber-reinforced cement composites. *Case Studies in Construction Materials*, 17:e01690.

[14] Lee, G.-W., Choi, Y.-C. (2022). Effect of abaca natural fiber on the setting behavior and autogenous shrinkage of cement composite. *Journal of Building Engineering*, 56:104719.

[15] Wijesinghe, K. A. P., Lanarolle, G., Gunasekara, C., Hidallana-Gamage, H. D., Law, D. W., Wang, L., Gamage, N., Gunathilaka, H. M. B. I. (2025). Thermal insulation and acoustic absorption performance of textile fibre-reinforced cement mortars. *Journal of Building Engineering*, 111:113128.

[16] Thien, D. V. H., Lam, D.-N., Diem, H. N., Pham, T. Y. N., Bui, N. Q., Truc, T. N. T., Van-Pham, D.-T. (2022). Synthesis of cellulose-g-poly(acrylic acid) with high water absorbency using pineapple-leaf extracted cellulose fibers. *Carbohydrate Polymers*, 288:119421.

[17] Lam, D.-N., Thien, D. V. H., Nguyen, C.-N., Nguyen, N. T. T., Viet, N. V., Van-Pham, D.-T. (2022). Thermally stable cellulose nanospheres prepared from office waste paper by complete removal of hydrolyzed sulfate groups. *Carbohydrate Polymers*, 297:120009.

[18] TCVN 2682:2020 (2020). *Portland cements*. Hanoi, Vietnam.

[19] TCVN 10302:2014 (2014). *Activity admixture - Fly ash for concrete, mortar and cement*. Hanoi, Vietnam.

[20] Lekhya, A., Kumar, N. S. (2024). A study on the effective utilization of ultrafine fly ash and silica fume content in high-performance concrete through an experimental approach. *Heliyon*, 10:e39678.

[21] Wang, S., Gu, X., Liu, J., Zhu, Z., Wang, H., Ge, X., Xu, X., Nehdi, M. L. (2023). Modulation of the workability and Ca/Si/Al ratio of cement-metakaolin cementitious material system by using fly ash: Synergistic effect and hydration products. *Construction and Building Materials*, 404:133300.

[22] El Inaty, F., Marchetti, M., Quiertant, M., Metalssi, O. O. (2024). Effect of curing on the coupled attack of sulfate and chloride ions on low-carbon cementitious materials including slag, fly ash, and metakaolin. *Construction and Building Materials*, 438:137307.

[23] Ylmén, R., Jäglid, U., Steenari, B.-M., Panas, I. (2009). Early hydration and setting of Portland cement monitored by IR, SEM and Vicat techniques. *Cement and Concrete Research*, 39:433–439.

[24] Nibou, D., Amokrane, S., Mekatel, H., Lebaili, N. (2009). Elaboration and characterization of solid materials of types zeolite NaA and faujasite NaY exchanged by zinc metallic ions Zn^{2+}. *Physics Procedia*, 2:1433–1440.

[25] Tesovnik, A., Ottosen, L. M., Ducman, V. (2025). Carbonation of lightweight alkali-activated aggregates based on biomass fly ash: Effect on microstructure and leaching behavior. *Case Studies in Construction Materials*, 23:e05014.

[26] Wei, G., Dong, B., Fang, G., Wang, Y. (2023). Understanding reactive amorphous phases of fly ash

through the acidolysis. *Cement and Concrete Composites*, 140:105102.
[27] He, M., Yang, Z., Li, N., Zhu, X., Fu, B., Ou, Z. (2023). Strength, microstructure, CO_2 emission and economic analyses of low concentration phosphoric acid-activated fly ash geopolymer. *Construction and Building Materials*, 374:130920.
[28] Zea-Garcia, J. D., Santacruz, I., Aranda, M. A. G., De la Torre, A. G. (2019). Alite-belite-ye'elimite cements: Effect of dopants on the clinker phase composition and properties. *Cement and Concrete Research*, 115:192–202.
[29] de Matos, P. R., Andrade Neto, J. S., Sakata, R. D., Kirchheim, A. P., Rodríguez, E. D., Campos, C. E. M. (2022). Strategies for XRD quantitative phase analysis of ordinary and blended Portland cements. *Cement and Concrete Composites*, 131:104571.
[30] Dana, K., Das, S., Das, S. K. (2004). Effect of substitution of fly ash for quartz in triaxial kaolin-quartz-feldspar system. *Journal of the European Ceramic Society*, 24:3169–3175.
[31] Lu, Q., Tang, L., Wang, S., Huang, B., Chen, Y., Chen, X. (2014). An investigation on the characteristics of cellulose nanocrystals from *Pennisetum sinese*. *Biomass and Bioenergy*, 70:267–272.
[32] Cheng, D., Jiang, S., Zhang, Q. (2012). Effect of hydrothermal treatment with different aqueous solutions on the mold resistance of moso bamboo with chemical and FTIR analysis. *BioResources*, 8:371–382.
[33] Wulandari, W. T., Rochliadi, A., Arcana, I. M. (2016). Nanocellulose prepared by acid hydrolysis of isolated cellulose from sugarcane bagasse. In *IOP Conference Series: Materials Science and Engineering*, 107:012045.
[34] Alemdar, A., Sain, M. (2008). Biocomposites from wheat straw nanofibers: Morphology, thermal and mechanical properties. *Composites Science and Technology*, 68:557–565.
[35] Zheng, D., Zhang, Y., Guo, Y., Yue, J. (2019). Isolation and characterization of nanocellulose with a novel shape from walnut (*Juglans regia* L.) shell agricultural waste. *Polymers*, 11:1130.
[36] Alzoubi, H. H., Albiss, B. A., Abu Sini, S. S. (2020). Performance of cementitious composites with nano PCMs and cellulose nano fibers. *Construction and Building Materials*, 236:117483.
[37] ASTM C348 (2021). *Standard test method for flexural strength of hydraulic-cement mortars*. ASTM International, West Conshohocken, PA, USA.
[38] ASTM C349 (2018). *Standard test method for compressive strength of hydraulic-cement mortars (using portions of prisms broken in flexure)*. ASTM International, West Conshohocken, PA, USA.
[39] Nguyen, M. H., Nguyen, V. T., Huynh, T.-P., Hwang, C.-L. (2021). Incorporating industrial by-products into cement-free binders: Effects on water absorption, porosity, and chloride penetration. *Construction and Building Materials*, 304:124675.
[40] Ventura-Cruz, S., Tecante, A. (2019). Extraction and characterization of cellulose nanofibers from Rose stems (*Rosa* spp.). *Carbohydrate Polymers*, 220:53–59.
[41] Bernard, E., Yan, Y., Lothenbach, B. (2021). Effective cation exchange capacity of calcium silicate hydrates (C-S-H). *Cement and Concrete Research*, 143:106393.
[42] Ahangaran, F., Hassanzadeh, A., Nouri, S. (2013). Surface modification of Fe_3O_4@SiO_2 microsphere by silane coupling agent. *International Nano Letters*, 3:23.
[43] Boudache, S., Loukili, A., Izoret, L., Rozière, E. (2023). Investigating the role played by portlandite and C-A-S-H in the degradation response of pozzolanic and slag cements to external sulphate attack. *Journal of Building Engineering*, 67:106053.
[44] Elsalamawy, M., Mohamed, A. R., Abosen, A. E. (2020). Performance of crystalline forming additive materials in concrete. *Construction and Building Materials*, 230:117056.
[45] Tang, H., Yu, J., Zhao, X. (2009). Controlled synthesis of crystalline calcium carbonate aggregates with unusual morphologies involving the phase transformation from amorphous calcium carbonate. *Materials Research Bulletin*, 44:831–835.
[46] Sahadat Hossain, M., Ahmed, S. (2023). Crystallographic characterization of naturally occurring aragonite and calcite phase: Rietveld refinement. *Journal of Saudi Chemical Society*, 27:101649.